Effects of constant electric fields on the buoyant stability of reaction fronts

A. Zadražil,[1] I. Z. Kiss,[2] J. D'Hernoncourt,[3] H. Ševčíková,[1] J. H. Merkin,[2] and A. De Wit[3]
[1]*Center for Nonlinear Dynamics of Chemical and Biological Systems, Prague Institute of Chemical Technology, Technicka 5, 166 28 Prague 6, Czech Republic*
[2]*Department of Applied Mathematics, University of Leeds, Leeds LS2 9JT, United Kingdom*
[3]*Service de Chimie Physique and Center for Nonlinear Phenomena and Complex Systems, Université Libre de Bruxelles, CP 231, Campus Plaine, 1050 Brussels, Belgium*
(Received 25 August 2004; published 8 February 2005)

The effects that applying constant electric fields have on the buoyant instability of reaction fronts propagating vertically in a Hele-Shaw cell are investigated for a range of electric field strengths and fluid parameters. The reaction produces a decrease in density across the front such that upwards propagating fronts are buoyantly unstable in the field-free situation. The reaction kinetics are modeled by cubic autocatalysis. A linear stability analysis reveals that a positive electric field increases the stability of a reaction front and can stabilize an otherwise unstable front. A negative field has the opposite effect, making the reaction front more unstable. Numerical simulations of the full nonlinear problem confirm these predictions and show the development of cellular fingers on unstable fronts. These simulations show that the electric field effects on the reaction within the front can alter the fluid density so as to give the possibility of destabilizing an otherwise stable downward propagating front.

DOI: 10.1103/PhysRevE.71.026224 PACS number(s): 89.75.Kd, 47.20.Bp, 82.40.Ck, 83.60.Np

I. INTRODUCTION

Propagating reaction-diffusion fronts develop in autocatalytic chemical systems from localized initiation sites. In such fronts, the unreacted state ahead is converted into a fully reacted state at the rear with the reaction being confined to a relatively narrow region. This change in reactant composition can change the density of the reactant mixture as the front propagates, thus giving rise to density gradients within the reaction zone. These density differences, though small, can set up buoyancy-driven convective flows, which, in turn, can destabilize the planar nature of the reaction front, leading to cellular fingering.

Systems based on the iodate-arsenous-acid (IAA) reaction have been shown to exhibit front waves and have been extensively studied experimentally in this context, see Ref. [1–3] for example. This reaction produces a decrease in density during the course of the reaction and hence upward-propagating fronts can become unstable to buoyancy effects. This has been observed experimentally in capillary tubes, see Ref. [4–6] for examples. An alternative way that has been proposed for visualizing buoyancy-driven instabilities is to use reactors based on the Hele-Shaw cell [7–10]. In these, the reaction takes place between two glass plates separated by a small gap of width h_0 (typically 1 mm or less) and mounted vertically in the present context. The region between the plates is filled with the reactant mixture and the reaction normally initiated by a horizontal line source along the reactor, usually in the form of a small current being applied to a strip electrode. Such a geometry allows for an easy experimental visualization of the spatially extended dynamics.

The advantage in using these Hele-Shaw reactors is that, for $h_0 \to 0$, the fluid dynamics can be described by a two-dimensional flow derived from the standard thin-film approximation to the Navier-Stokes equations, effectively Darcy's law, together with equivalent equations for the reactants. This simplifies the modeling and the analytic description of any buoyancy-driven instabilities. This simplification has been exploited recently using a reduced model for the iodate-arsenous-acid reaction [11,12] and for the chlorite-tetrathionate (CT) reaction [13,14]. In both cases the effect of the convective flow was characterized by a Damköhler number and, for increasing values of this parameter, a planar reaction front became more unstable to transverse perturbations (identified through a linear stability analysis) with cellular fingers developing as the reaction proceeded.

Previous studies [15–19] have shown that applying an electric field to an ionic autocatalytic system alters both the propagation speed of the reaction front and the final outcome of the reaction. This latter effect changes the density from what it would otherwise have been both within the reaction region and at the rear of the wave. This, in turn, has the effect of modifying the induced convection flow and thus the stability of the reaction fronts. In this paper, we consider the effect of applying constant planar electric fields to reaction fronts propagating vertically within a Hele-Shaw reactor. This work is motivated by an experimental study of this system [20] which used the iodate-arsenous-acid reaction with the arsenous acid being in excess. These experiments showed that applying an electric field through plate electrodes mounted at the top and bottom of the reactor could either increase or reduce the buoyant instability, depending on the polarity of the electrodes. The ability of applied electric fields to radically change the propagation of reaction-diffusion waves by changing the density gradients has been clearly demonstrated in Ref. [21] for pulse waves propagating horizontally in a Belousov-Zhabotinsky (BZ) system.

Our aim here is to describe how constant electric fields influence the buoyant stability of vertically propagating fronts by considering a simplified generic model of reaction-diffusion front. We use cubic autocatalysis for the kinetics.

We have already shown that this is a good approximation for the full Dushman-Roebuck scheme in the arsenous-acid excess case [22]. We assume a high ionic strength for the reaction mixture (consistent with the experiments) and a constant electric field enabling simplifications to be made in modeling the electric field effects. For the fluid flow in the Hele-Shaw cell we use Darcy's law including a term representing the buoyancy forces. Based on this model, we perform a linear stability analysis of our model to show that applying constant electric fields can have opposite effects, both stabilizing an otherwise unstable configuration as well as strengthening the buoyant instabilities. This is borne out in our numerical simulations of the full model.

Reaction fronts in systems based on cubic autocatalysis can also sustain diffusional instabilities, provided the mass transfer of the autocatalyst is somewhat less than that of the substrate [23]. This is not the case for the iodate-arsenous-acid reaction (and so will not be part of our model) unless some complexing agent is used to bind with the autocatalyst, starch [24] and α-cyclodextrin [25] being used in experiments. The effect of applying an electric field to these diffusional instabilities has been examined in Refs. [26,27], where it was shown that electric fields can either stabilize or magnify the instability in this situation as well.

This paper is organized as follows. First we define the system studied and derive a dimensionless mathematical model for it. Then we consider the planar traveling wave solutions to our model in the absence of hydrodynamical flow in order to assess the effects of constant electric fields on the velocity and the concentration profile of pure reaction-diffusion fronts. These traveling wave solutions are subjected to a linear stability analysis in the next section. The effects of both the buoyant and electric forces on upward-propagating fronts are determined through dispersion relations giving the dependencies of growth rates on wave numbers. Finally, we solve the full mathematical model numerically in order to test the predictions of the linear stability analysis and to follow the nonlinear development of front instability from an originally flat front. In our numerical studies, the development of both upward- and downward-propagating fronts is analyzed.

II. MATHEMATICAL MODEL

Our model is based on the experiments on the effects that constant electric fields can have on the buoyant stability of reaction fronts in the IAA system in a Hele-Shaw cell [20]. We have previously established that, in the arsenous acid excess case, the iodate-arsenous acid reaction can be represented to a good approximation by cubic autocatalysis [22]. This leads us to take

$$A^- + 2B^- \rightarrow 3B^- \quad \text{rate } k_0 ab^2 \tag{1}$$

for our kinetics, where A^- and B^- represent, respectively, IO_3^- and I^-, with concentrations a and b, and k_0 is the rate constant.

The Hele-Shaw reactor is mounted vertically, with the x axis measuring distance in the upward vertical direction and y horizontally across the cell. The electric field is taken to be

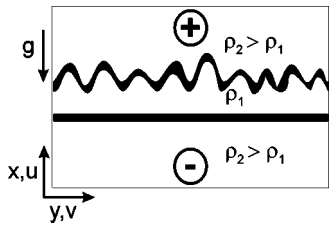

FIG. 1. Schematic representation of the system.

planar acting in the x direction with the polarity, for positive field strengths, as indicated in Fig. 1, i.e., the effect of a positive electric field is to increase the transport of the negative ions in the positive x direction. The equations for our two-dimensional model system are derived from the standard thin-film equations (lubrication theory) [28] for the fluid flow together with reaction-diffusion-advection equations for the concentrations, also derived using the thin-film approximation, namely

$$\frac{\partial u}{\partial x} + \frac{\partial v}{\partial y} = 0, \tag{2}$$

$$\frac{\partial p}{\partial x} = -\frac{\mu}{K}u - g\rho(a,b), \tag{3}$$

$$\frac{\partial p}{\partial y} = -\frac{\mu}{K}v, \tag{4}$$

$$\frac{\partial a}{\partial t} + u\frac{\partial a}{\partial x} + v\frac{\partial a}{\partial y} + D_A\mathcal{E}\frac{\partial a}{\partial x} = D_A\left(\frac{\partial^2 a}{\partial x^2} + \frac{\partial^2 a}{\partial y^2}\right) - k_0 ab^2, \tag{5}$$

$$\frac{\partial b}{\partial t} + u\frac{\partial b}{\partial x} + v\frac{\partial b}{\partial y} + D_B\mathcal{E}\frac{\partial b}{\partial x} = D_B\left(\frac{\partial^2 b}{\partial x^2} + \frac{\partial^2 b}{\partial y^2}\right) + k_0 ab^2, \tag{6}$$

together with an "equation of state"

$$\rho(a,b) = \rho_0 + \gamma_1 a + \gamma_2 b, \tag{7}$$

where $\rho_0 = \rho(0,0)$ is the fluid density without the reactants A^- and B^- and $\gamma_{1,2}$ are the positive solutal expansion coefficients of species A and B. In the above, the pressure p is independent of the distance across the gap. The velocity components u and v (in the x and y directions, respectively) and the concentrations a and b are their values averaged across the gap, following the standard derivation of the equations for a Hele-Shaw cell. ρ is the density, g is the acceleration due to gravity, μ is the viscosity of the fluid, and K the permeability, related to the thickness h_0 of the cell by $K = h_0^2/12$. D_A and D_B are the diffusion coefficients of reactants A^- and B^- and $\mathcal{E}$ is the (constant) electric field strength, on making the constant field approximation, the validity of which is discussed in Ref. [19].

We make Eqs. (2)–(7) dimensionless by introducing the time T_0, length L_0, and velocity U_0 scales

$$T_0 = \frac{1}{k_0 a_0^2}, \quad L_0 = \left(\frac{D_A}{k_0 a_0^2}\right)^{1/2}, \quad U_0 = \frac{g\Delta\rho K}{\mu}, \tag{8}$$

with a_0 being the initial concentration of A^-, $\Delta\rho=(\rho_r-\rho_p)$, where $\rho_r=\rho_0+\gamma_1 a_0$ and $\rho_p=\rho_0+\gamma_2 a_0$ are the *field-free* densities of the reactant and product solutions, respectively, i.e., $\Delta\rho=(\gamma_1-\gamma_2)a_0$. We then write

$$(u,v) = U_0(\overline{u,v}), \quad (x,y) = L_0(\overline{x,y}),$$

$$t = T_0\overline{t}, \quad p = \frac{\mu U_0 L_0}{K}\overline{p}, \quad (a,b) = a_0(\overline{a},\overline{b}). \tag{9}$$

In addition, we scale the density as $\overline{\rho}=\rho/\Delta\rho$ and define

$$\overline{\gamma_1} = \frac{\gamma_1 a_0}{\Delta\rho}, \quad \overline{\gamma_2} = \frac{\gamma_2 a_0}{\Delta\rho} \quad \left(\text{so that } \frac{\overline{\gamma_1}}{\overline{\gamma_2}} = \frac{\gamma_1}{\gamma_2}\right). \tag{10}$$

This leads to the dimensionless equations for our model as, on dropping the bars for convenience,

$$\frac{\partial^2\psi}{\partial x^2} + \frac{\partial^2\psi}{\partial y^2} = -\left(\gamma_1\frac{\partial a}{\partial y} + \gamma_2\frac{\partial b}{\partial y}\right), \tag{11}$$

$$\frac{\partial a}{\partial t} + \beta\left(\frac{\partial\psi}{\partial y}\frac{\partial a}{\partial x} - \frac{\partial\psi}{\partial x}\frac{\partial a}{\partial y}\right) = \left(\frac{\partial^2 a}{\partial x^2} + \frac{\partial^2 a}{\partial y^2}\right) - E\frac{\partial a}{\partial x} - ab^2, \tag{12}$$

$$\frac{\partial b}{\partial t} + \beta\left(\frac{\partial\psi}{\partial y}\frac{\partial b}{\partial x} - \frac{\partial\psi}{\partial x}\frac{\partial b}{\partial y}\right) = D\left(\frac{\partial^2 b}{\partial x^2} + \frac{\partial^2 b}{\partial y^2}\right) - DE\frac{\partial b}{\partial x} + ab^2, \tag{13}$$

where we have introduced the stream function ψ, defined in the usual way, and eliminated the pressure from the equations. Here

$$D = \frac{D_B}{D_A}, \quad \beta = \frac{T_0 U_0}{L_0} = \frac{g\Delta\rho K}{\mu(D_A k_0 a_0^2)^{1/2}}, \quad E = \left(\frac{D_A}{k_0 a_0^2}\right)^{1/2}\mathcal{E}. \tag{14}$$

Initially $a=1$, $b=0$, and $\psi=0$ (no flow) with a local input of B^- applied horizontally across the reactor to start the reaction. When the density jump $\Delta\rho$ across the front is zero, $\beta=0$ and we recover the pure reaction-diffusion system in the presence of the electric field. When $\Delta\rho$ is increased, β increases and we can then analyze the influence of buoyancy-induced convective flows and their coupling with the applied electric field. For the iodate-arsenous acid reaction, the density of the product after the passage of the wave is less than the initial reactants, at least when no electric field is applied [4,5]. From this it follows that $\gamma_1>\gamma_2$ and the change in density resulting from the reaction ($\Delta\rho>0$) means that *upward*-propagating waves can become buoyantly unstable through a Rayleigh-Taylor instability.

Reaction (1) converts all A^- ahead of the front to B^- behind the front leaving the product at the concentration $b=b_s$. This concentration is dependent on both the electric field strength and the ratio of diffusion coefficients D [29], with, in general, $b_s\neq 1$.

III. TRAVELING WAVES

To consider the planar propagating reaction fronts, we introduce the traveling coordinate $\zeta=x-ct$, where c is the (constant) wave speed. This leads to the traveling wave equations, in the absence of flow ($\beta=0$),

$$a'' + (c-E)a' - ab^2 = 0, \quad Db'' + (c-DE)b' + ab^2 = 0 \tag{15}$$

(where primes denote differentiation with respect to ζ) subject to

$$a\to 1,\ b\to 0 \quad \text{as } \zeta\to\infty, \quad a\to 0,\ b\to b_s \quad \text{as } \zeta\to-\infty, \tag{16}$$

where b_s is a constant to be determined and will depend on E and D. The reaction terms can be eliminated by adding Eqs. (15) with the resulting equation integrated to get

$$a' - (c-E)(1-a) + Db' + (c-DE)b = 0. \tag{17}$$

Expression (17) enables us to determine a relation between b_s and the wave speed c,

$$b_s = \frac{c-E}{c-DE} = 1 + \frac{(D-1)E}{c-DE} \tag{18}$$

with c having to be determined from the solution of Eqs. (15) and (16).

Equations (15)–(17) have been examined in detail in Ref. [29], where it was shown that, for $D\neq 1$, the existence of a solution is limited by the field strength, by positive fields for $D<1$ and by negative fields if $D>1$. For $D=1$, the equations have an analytic solution, giving $c=1/\sqrt{2}+E$ and no limit on the field strength for the existence of traveling waves. A typical plot of the wave speed c against E for $D>1$ is shown in Fig. 2 (in this case for $D=2.0$). Also shown in the figure is b_s. Note that, from Eq. (18), $b_s>1$ for $E>0$ and $b_s<1$ for $E<0$. A value of the field strength $E=E_0=-1/D\sqrt{2}$ was also found at which the reaction front became stationary, i.e., $c=0$. There is also, for $D>1$, a lower bound E_c on E for the existence of waves. For $D=2$, $E_c=-0.355$ with $c<0$ for $E_c<E<E_0$. There is no restriction on positive field strengths for the existence of waves with, for $D=2$,

$$c \sim 2E + 1.140E^{1/3} + \cdots, \quad b_s \sim 1 + 0.877E^{2/3} + \cdots \quad \text{as } E\to\infty.$$

In Ref. [29] it was shown that, when traveling waves did not exist, i.e., $E<E_c$ when $D>1$, complete electrophoretic separation of A^- and B^- developed, with then no reaction between these species.

IV. LINEAR STABILITY ANALYSIS

To consider the stability of the reaction fronts to a Rayleigh-Taylor instability, we put

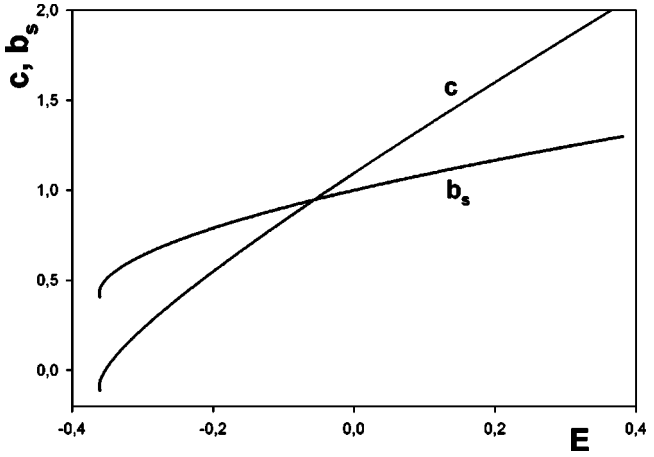

FIG. 2. Speed c of the traveling fronts and autocatalyst concentration b_s at the rear of the front, against E for $D=2.0$, obtained from a numerical integration of Eqs. (15) and (16).

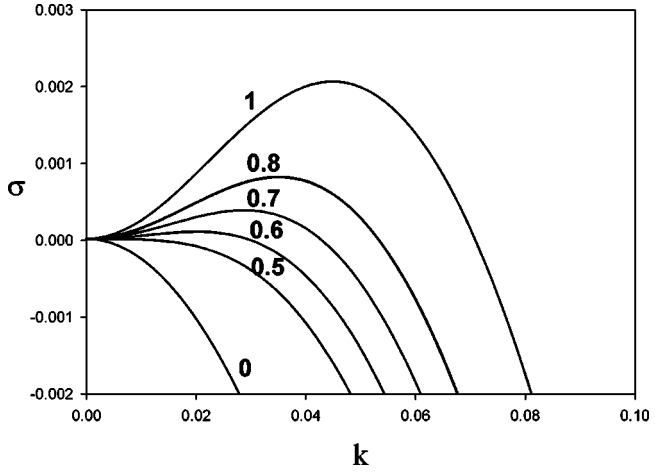

FIG. 3. Dispersion curves for the field-free ($E=0$) case for a range of values of β with $D=2.0$, $\gamma_1=1$, and $\gamma_2=0.5$.

$$a(\zeta,y,t) = a_0(\zeta) + A(\zeta,y,t),$$

$$b(\zeta,y,t) = b_0(\zeta) + B(\zeta,y,t), \tag{19}$$

where $a_0(\zeta)$ and $b_0(\zeta)$ are the traveling wave solutions discussed in the previous section and take A,B and $\psi = \psi(\zeta,y,t)$ to be small perturbations. We substitute Eqs. (19) into Eqs. (11)–(13) and look for a solution in the form

$$A(\zeta,y,t) = \mathrm{e}^{\sigma t+iky}A_0(\zeta),$$

$$B(\zeta,y,t) = \mathrm{e}^{\sigma t+iky}B_0(\zeta), \tag{20}$$

$$\psi(\zeta,y,t) = \mathrm{e}^{\sigma t+iky}\psi_0(\zeta).$$

This leads to an eigenvalue problem for (A_0,B_0,ψ_0) in terms of the growth rate σ and the wave number k as

$$A_0'' + (c-E)A_0' - (b_0^2 + k^2 + \sigma)A_0 - 2a_0b_0B_0 - \beta a_0'u_0 = 0, \tag{21}$$

$$DB_0'' + (c-DE)B_0' - (Dk^2 - 2a_0b_0 + \sigma)B_0 + b_0^2A_0 - \beta b_0'u_0 = 0, \tag{22}$$

$$u_0'' - k^2u_0 - k^2(\gamma_1A_0 + \gamma_2B_0) = 0, \tag{23}$$

where we have put $u_0 = ik\psi_0$, subject to

$$A_0 \to 0, \quad B_0 \to 0, \quad u_0 \to 0 \quad \text{as } |\zeta| \to \infty. \tag{24}$$

Equations (21)–(24) were solved numerically using the technique described in Refs. [13,14]. The method involves discretizing Eqs. (21)–(23) together with Eqs. (15) using central-difference approximations for the derivatives. This enables the system to be written as a matrix eigenvalue problem, which was solved using the LAPACK solver DGEEVX [30]. From these calculations, the largest eigenvalue σ is determined for increasing values of the wave number k and these are the values plotted on the dispersion curves presented below. A large number of grid points for the computational domain and accurate representations of the traveling wave solutions at their front and rear, where the perturbations from the corresponding boundary conditions are exponentially small, are required for an accurate calculation of the largest eigenvalues. The number of grid points N used in these calculations was dependent on the context, essentially the width of the planar reaction front. N varied from $N=420$ to $N=750$, with a grid spacing $\Delta\zeta=0.1$ being used in each case.

Without an electric field, our model system can have a purely diffusional instability (no flow, $\beta=0$). This requires $D<1$ following the argument given in Ref. [23]. Our numerical calculations of the eigenvalues σ with $\beta=0$, $E=0$ confirm that this is the case. We find that there is a critical value of D between $D=0.5$ and $D=0.4$ for the onset of a diffusional instability [32], which is in agreement with the critical value of $D=0.435$ reported previously [26,33].

Our study is motivated by experiments with the iodate-arsenous acid reaction for which $D>1$ [31], and so we will not get a diffusional instability in our case. We took $D=2.0$ as being a representative value. The aim of our linear stability analysis from Eqs. (21)–(24) is to consider how the hydrodynamic flow (through the parameter β) and the electric field E affect the transverse stability of the traveling waves. For this we take a value for the ratio $\gamma_2/\gamma_1=0.5$ as being representative [34]. Here we are concerned with the stability of upward-propagating fronts. For downward-propagating fronts, the sign of the buoyancy force term in Eq. (11) has to be changed to perform the linear stability analysis. We started by considering the field-free ($E=0$) case. The results are shown in Fig. 3 with dispersion curves for different values of β. The figure shows that $\sigma<0$ for all $k>0$ when $\beta=0$, as expected, and that the strength of the instability (larger values for the maximum value of σ and a greater range of unstable wave numbers) becomes more pronounced as β is increased.

To assess the effect that applying an electric field has on the buoyant stability of the reaction fronts, we took given values of $\beta=1.0$, $D=2.0$, $\gamma_1=1$, and $\gamma_2=0.5$ and computed the dispersion curves for a range of field strengths E. The results are shown in Fig. 4(a) for upward-propagating fronts.

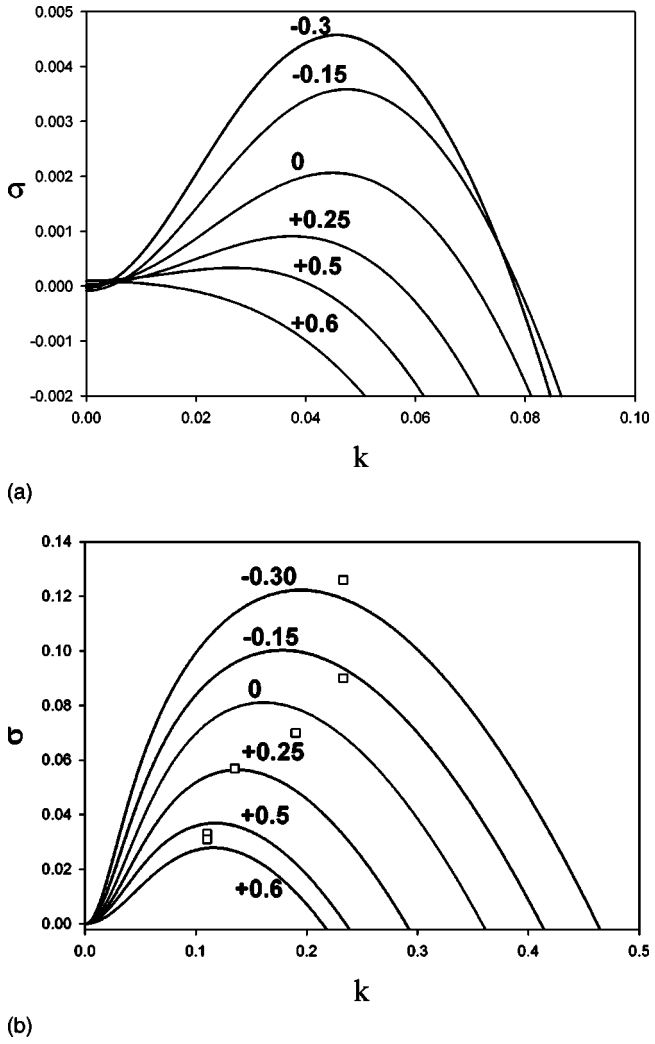

FIG. 4. Dispersion curves for upward-propagating fronts for $D=2.0$, $\gamma_1=1$, and $\gamma_2=0.5$ for the positive and negative field strengths indicated in the figure, with (a) $\beta=1.0$ and (b) $\beta=5.0$. The squares indicate the most unstable mode as obtained from the nonlinear simulations.

This figure shows that the effect of applying a positive field (in the sense defined in Fig. 1) is to make the reaction fronts more stable (decrease the maximum value of σ and the range of unstable wave numbers) and, for a sufficiently strong field, to stabilize the wave. In Fig. 4(a) we see that, for $\beta=1.0$, the wave is marginally unstable with $E=0.5$ and fully stable at $E=0.6$. The effect of negative fields, where the induced transport of the negative ions is in the opposite sense to the direction of propagation, is to make the reaction front more unstable. For example, Fig. 4(a) shows a considerable increase in the maximum value of σ (and an increase in the range of unstable wave numbers) for $E=-0.3$ over what it would be for $E=0$. Note that there are no traveling waves for negative field strengths greater than $|E|=0.355$ and this is the limit of the stability analysis.

To consider the effect of the flow parameter β on the stability of the traveling waves, we took a larger value $\beta=5.0$ for this parameter and computed the dispersion curves for the same field strengths as used in Fig. 4(a). The results are shown in Fig. 4(b). This figure shows that a stronger flow makes the waves much more unstable, with all the waves being unstable (for both positive and negative field strengths) in this case. The maximum value for σ and the range of unstable wave numbers is at least an order of magnitude greater for $\beta=5$ than for $\beta=1$.

V. NUMERICAL SIMULATIONS

To test the predictions of the linear stability analysis and gain insight into the nonlinear dynamics of the system, we solved Eqs. (11)–(13) numerically using a pseudospectral code as described in Refs. [12–14,35]. The modification to this program was to add in (linear) terms to account for the transport of the negative ions in the applied electric field. This numerical scheme is based on Fourier expansions for the stream function ψ and concentrations a and b. The result is sets of time-dependent ordinary differential equations for the Fourier coefficients, which are integrated using the Adams-Bashforth method. The integration was performed on a uniform spatial grid of size $\Delta x=\Delta y=1$ and a time step typically of order $\Delta t=0.04$. The numerical simulations were started with $a=1$ and $b=0$ everywhere except in a central horizontal strip where $a=0$ while b was set to $b=1$ to start the reaction. Noise of 0.1% amplitude was added to the front to initiate the instabilities. This procedure allows both an upward- and a downward-propagating wave to develop and directly follows the experimental procedure [20]. The course of the reaction is monitored by gray-level plots of the concentrations of reactant A^- and the autocatalyst B^- ranging from 0 (white) to 1 or b_s (black) for a and b, respectively. We first checked that, in the absence of any flow, the numerical procedure recovers the reaction-diffusion traveling waves as well as the correct influence of E both on the shape and speed of the waves as described in Ref. [29]. We then investigated the Rayleigh-Taylor instability of such fronts. To do so, we took $\beta=5.0$, so as to get a strongly developing instability, still with $D=2.0$ and took $\gamma_1=1$, $\gamma_2=0.5$.

We started with the field-free case ($E=0$). The results are shown in Fig. 5 by gray-level plots of a at increasing times in a system of dimensionless width 512. The aspect ratio between the x and y directions is preserved in the plots. Small-amplitude disturbances develop on the upward-propagating front, initially having small wavelengths. These disturbances grow in size, coalescing as they do so, to produce large-amplitude cellular fingers seen previously [12,13]. Our results are consistent with those reported in Ref. [12] for the IAA system and in Ref. [13] for the CT system, except in this latter case it is the downward-propagating front that becomes unstable rather than the upward-propagating front in the IAA system because of the different change in density resulting from the reaction.

We next considered the effect of applying a given positive or negative electric field (in the sense described in Fig. 1). To check the linear stability analysis, we compared the most unstable mode observed in the nonlinear simulation with the one predicted by the dispersion curves. To do so, we integrated the nonlinear model for various values of E in wide systems such that at least 20 fingers appear at onset. We then

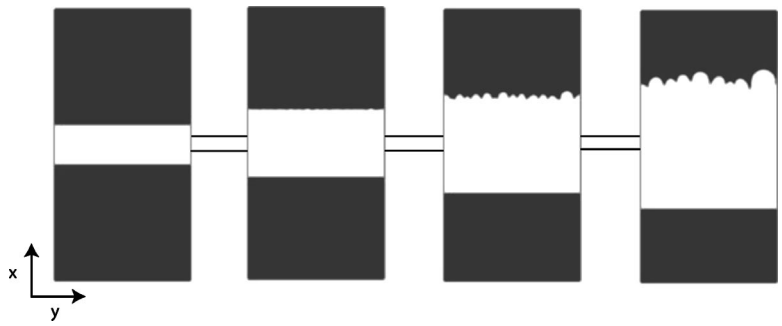

FIG. 5. Gray-level plots of a in the field-free case ($E=0$) at times $t=50$, 100, 150, and 200, with $\beta=5.0$, $D=2.0$, $\gamma_1=1$, and $\gamma_2=0.5$. The horizontal lines indicate the initial position of the fronts. Gray levels range from white ($a=0$) to black ($a=1$). In the absence of an electric field, only the upward-propagating front is unstable.

computed the most unstable wave number $k_m=2\pi/\lambda$ and its growth rate $\sigma=2\pi/T$ where λ is the wavelength of the pattern and T the time when fingering becomes visible on the gray scale plots of concentration a. These values are shown in Fig. 4(b) (by the solid squares) and can be seen to be in good agreement with the linear stability predictions.

With $E=+0.3$, both upward- and downward- (corresponding to having $E=-0.3$) propagating fronts form. The results are shown in Fig. 6 with gray-level plots of a and b taken at $t=200$. This figure shows that an instability develops on the upward-propagating front, having a similar form to that seen when $E=0$, though it takes a little longer for it to develop and the resulting cellular fingers are a little less pronounced (compare with Fig. 5 at $t=200$). Thus the nonlinear simulations confirm that the upward-moving front is becoming stabilized by the positive electric field as predicted by the linear stability analysis. This can be understood by inspecting the transverse averaged profiles of the concentrations a,b and of the dimensionless density excess of the solution with regard to water $\rho-\rho_0=\gamma_1 a+\gamma_2 b$ (shown in Fig. 7). When E is positive, the reaction-diffusion front speed c is larger (see Fig. 2) and so the upward-moving front travels faster than the purely reaction-diffusion ($E=0$) case. The downward-propagating

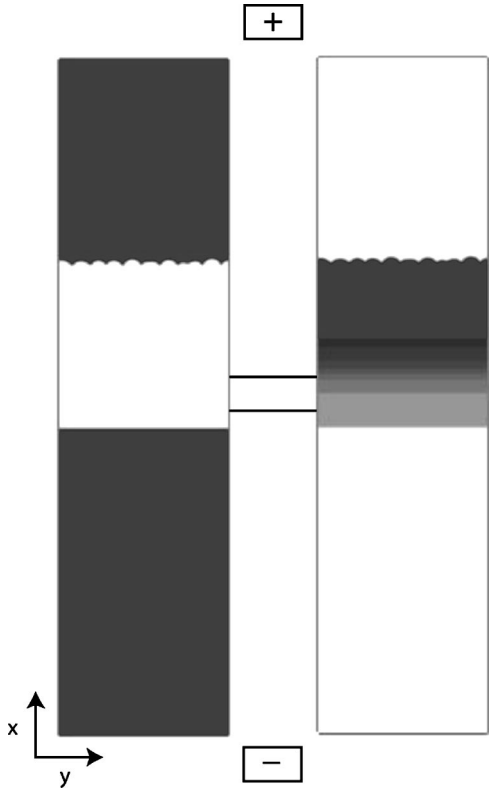

FIG. 6. Gray-level plots of a and b for $E=+0.3$ at time $t=200$, with $\beta=5.0$, $D=2.0$, $\gamma_1=1$, and $\gamma_2=0.5$. The horizontal lines indicate the initial position of the fronts. Gray levels range from white ($a=b=0$) to black ($a=1$; $b=b_s$). For this positive value of E, the upward-moving front is more stable than in the field-free case.

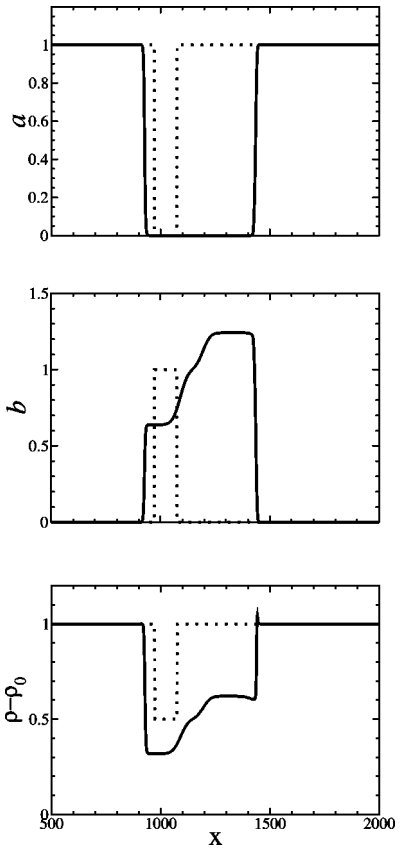

FIG. 7. Transverse averaged profiles of concentrations a,b and of the density excess $\rho-\rho_o$ at time $t=200$ corresponding to the gray-level plots shown in Fig. 6. The dotted curve is the initial condition.

front (for which, in effect, $E<0$) has a smaller speed than the purely reaction-diffusion case. This larger speed of the upward-moving front more efficiently opposes the development of the hydrodynamic instability [11], making it more stable.

We can also gain some idea as to why stabilization occurs by considering the (dimensionless) density jump $\delta\rho$ across the upward-moving front in the presence of an electric field,

$$\delta\rho(E) = \gamma_1 - \gamma_2 b_s(E), \tag{25}$$

with a necessary condition for buoyant instability of the upward-propagating front being $\delta\rho>0$. As b_s is an increasing (decreasing) function for positive (negative) electric fields (see Fig. 2), it follows that applying a positive electric field increases the value of b_s behind the upward-moving front and thus reduces the effective density jump across the front, effectively stabilizing the system. For the present case $b_s=1.241$, giving $\delta\rho=0.379$, less than the field-free case for which $\delta\rho=0.5$. As a corollary, the density jump increases for negative E and so the descending fronts are made more stable. This can clearly be seen in the density profiles [Fig. 7(c)]. In this figure, gravity is acting towards small values of x and the top of the cell corresponds to large x. The upward-moving front has a smaller density jump than the initial condition (plotted as a dotted line). This explains why the upward-moving front is more stable than in the field-free case. The downward front still has less dense solution above a heavier one, which is a stable situation. Note that the tiny peak, for which $\rho>1$, in Fig. 7(c) results from the fact that $D>1$ and so b diffuses more quickly than a. Hence the front in b is slightly wider than that in a, leading to a small area of higher ρ ahead of the front. This small excess is not large enough to trigger any fluid motion.

Between the two reaction fronts, an electrophoresis front in b also develops [29] through which the difference in the concentration of b at the rear of the upward- and downward-propagating reaction fronts is adjusted [see Fig. 7(b)]. This gives a local change in density $\delta\rho_e$ across the electrophoretic front,

$$\delta\rho_e = \gamma_2(b_s^+ - b_s^-), \tag{26}$$

where b_s^+ and b_s^- are the concentrations of b at the rear of the upward- and downward-propagating fronts, respectively. In the present case, this local change in density between the two fronts does not lead to further instabilities. Figure 7 indicates the formation of the electrophoresis front and shows that the transition in the concentration of b is smoother than in the much sharper reaction fronts, consistent with the results given in Ref. [29]. As smooth fronts are more stable than sharp ones [11], this could well account for why this density change is not driving an instability.

We then considered negative fields, starting with $E=-0.3$. With respect to just the reaction-diffusion fronts, this change of sign has the effect only of changing the speed of propagation of the fronts considered previously with now the downward-moving front traveling faster. Gray-level plots of a and b at $t=200$ are given in Fig. 8. The effect of the flow is to make the upward-propagating front much more unstable (compare with Fig. 5 at the same time). This is due to the fact that the front travels slower and now there is a greater change in density $\delta\rho$ across the front. From the traveling wave solutions, $b_s=0.638$, giving $\delta\rho=0.681$ for this case. Note that here there is a positive density change across the electrophoresis front (see Fig. 9). This has the effect of "confining" the stronger convection flow behind the upward-propagating front and thus further enhancing its destabilizing effect on the upward propagation of the reaction. This is indicated in Fig. 9, where the transverse averaged profiles are plotted, suggesting that the reaction takes place within a relatively narrow region with the effects of the flow generated by the buoyant instability being felt at considerable distances (ahead for a and behind for b) from the reaction zone.

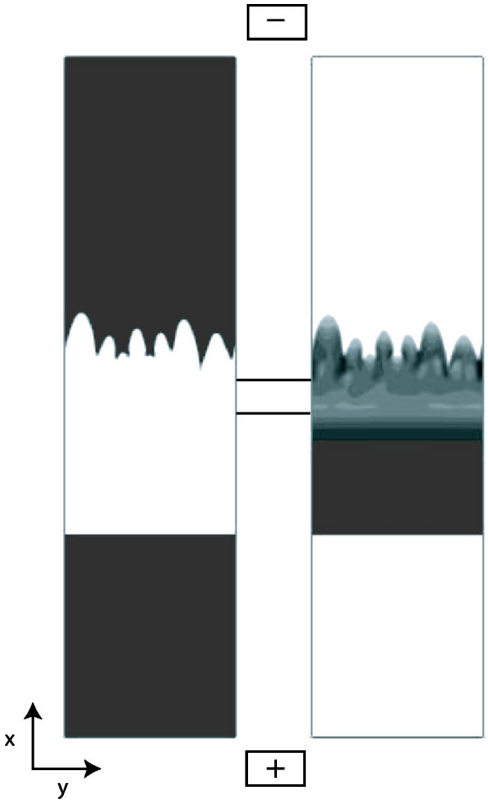

FIG. 8. Gray-level plots of a and b for $E=-0.3$ at time $t=200$, with $\beta=5.0$, $D=2.0$, $\gamma_1=1$, and $\gamma_2=0.5$. The horizontal lines indicate the initial position of the fronts. Gray levels range from white ($a=b=0$) to black ($a=1$; $b=b_s$). For this negative value of E, the upward-moving front is more unstable than in the field-free case.

We then took a higher value for the negative field, taking $E=-1.0$. In this case, there is no upward-propagating reaction front (see Fig. 2) and the concentrations of a and b form distinct electrophoresis fronts [29]. The results of the numerical simulation at $t=200$ are shown in Fig. 10. The total separation of the reacting species on the upper front is clearly seen in the figure. The front in a becomes unstable with large-scale cellular fingers having formed by this time. The front in b is stable. The situation in this case is similar to cellular fingers arising on an interface between nonreactive fluids of different densities (see Refs. [36,37] for example) though here the density change is caused by the concentrations of the reaction species and the interface is moving downwards with a constant speed ($|E|$ for a and $D|E|$ for b

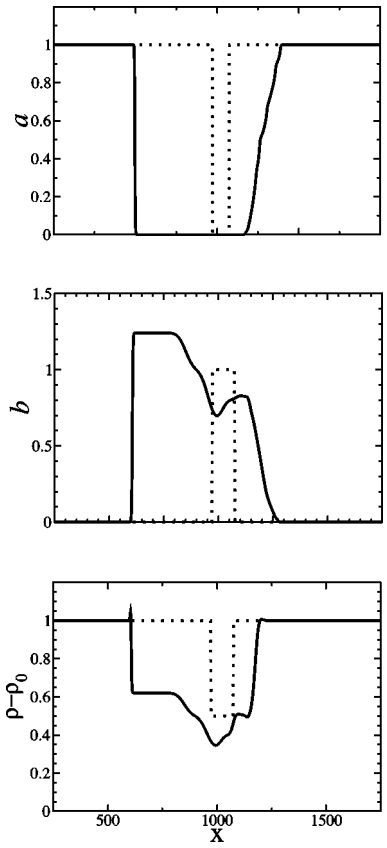

FIG. 9. Transverse averaged profile of concentrations a, b and of the density excess $\rho-\rho_o$ at time $t=200$ corresponding to the gray-level plots shown in Fig. 8.

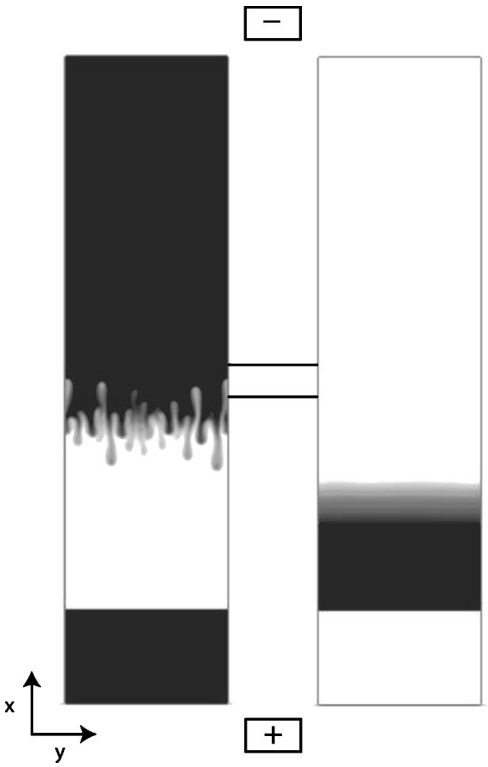

FIG. 10. Gray-level plots of a and b for $E=-1.0$ at time $t=200$, with $\beta=5.0$, $D=2.0$, $\gamma_1=1$, and $\gamma_2=0.5$. The horizontal lines indicate the initial position of the fronts. Gray levels range from white ($a=b=0$) to black ($a=1$; $b=b_s$). For this larger negative value of E, there is a total separation of the reacting species on the upper front. The upper electrophoretic front in a is the only one to be unstable.

[29]). Since there is a positive density change only for the upper front of a (see the profiles in Fig. 11), this is the only front on which an instability can occur. Note also in Fig. 11 that the large-scale fingering is witnessed by the presence of bumps in the transverse averaged profiles of a [12], which leads to nonmonotonous changes in the density profile.

Eventually, for strongly negative electric field, $E=-3.0$ for instance (Fig. 12), we are still in the electrophoretic regime but the value of b_s becomes sufficiently large for the density jump to be positive both for the upper electrophoresis front in a and for the lower reaction front in a and b (Fig. 13). As a consequence, both these fronts show the development of density fingering, though with very different characteristics. The cellular fingering seen in the electrophoresis front is similar to that seen in Fig. 10 (for $E=-1.0$) but is plotted here at a later time ($t=300$) for which fingering is a little more vigorous, as can be seen in the profile plots in Fig. 13, especially in the density plot. The instability on the (downward-propagating) reaction front is relatively weak at this field strength and cellular fingering has not become fully established by this time.

So far we have considered the fixed values of $\gamma_1=1$, $\gamma_2=0.5$ and have seen that varying the intensity of the electric field can alter the stability of both reaction and electrophoretic fronts. It is clear that the stability of a reaction front depends essentially on the density jump $\delta\rho=\gamma_1-\gamma_2 b_s$ across it. For a fixed value of the electric field, we can expect a change of stability for the critical value of the ratio $\gamma_2/\gamma_1=1/b_s$. For fixed chemical species, γ_2/γ_1 is constant and a change of stability can be triggered by the variation of the electric field changing the final product concentration and thus the density of the fluid after the passage of the front, as we have shown. For a fixed E, depending on the relative values of γ_1 and γ_2, the stability characteristics can be different. Here all results have been presented for $\gamma_2/\gamma_1=0.5$. If γ_2/γ_1 is decreased, the various stability changes we have described above will be observed for smaller $|E|$. A change of stability of electrophoretic fronts cannot be reached by changes of the ratio γ_2/γ_1, as seen by considering expression (26) for the density jump $\delta\rho_e$. Only the magnitude of the instability depends in that case on the expansion coefficients.

Finally, we note that we have focused on a reaction for which the reactants are heavier than the products ($\gamma_1>\gamma_2$) such as in the IAA reaction. Generalization of our results to the case of reactions where the density increases in the course of reaction ($\gamma_1<\gamma_2$), as it does in the CT reaction, for example, is straightforward.

VI. DISCUSSION

We have considered the effects that applying a constant electric field can have on the stability of reaction fronts

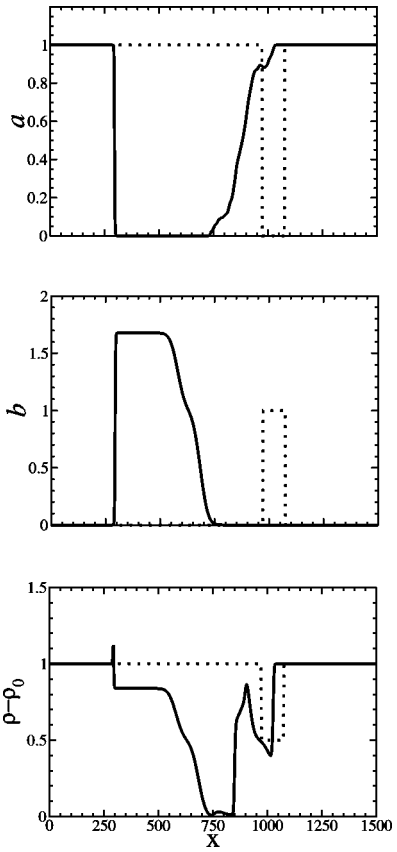

FIG. 11. Transverse averaged profile of concentrations a, b and of the density excess $\rho-\rho_o$ at time $t=200$ corresponding to the gray-level plots shown in Fig. 10.

propagating vertically within a Hele-Shaw cell in a cubic autocatalytic system for which the density decreases across the front. We have been concerned only with buoyancy-induced instabilities arising from the natural convection flow set up by changes in fluid density resulting from the passage of a reaction front. We have seen that a positive electric field, in the sense described in Fig. 1, has the effect of stabilizing the upward-moving front, whereas a negative field magnifies the instability by increasing the growth rate and the range of unstable wave numbers (Fig. 4). Numerical integrations of the full nonlinear problem, starting with a localized (strip) input of autocatalyst, show the development of large-scale cellular fingers from the initially small-scale perturbations in concentration in cases when the system is unstable. The extent and rate of growth of these fingers is strongly influenced by the electric field, compare Fig. 5 for the field-free case with Fig. 6 for a positive field (weaker growth) and Figs. 8, 10, and 12 for negative fields (much stronger growth).

The decrease in fluid density resulting from the autocatalytic reaction (1) means that, in general, it is only upward-propagating fronts that become unstable, with downward-propagating fronts remaining stable (Figs. 5, 6, and 8). This is the case for relatively weak fields. For stronger (negative) fields, upward-propagating fronts cannot form (see Fig. 2) and separate electrophoresis fronts in A^- and B^- develop, with the front in B^- traveling faster than that in A^-. This leaves a region where there are no reactants and in this region the density is purely that of the solvent (water), having a lower density than the initial density when some A^- is present. This density change (heavy fluid above lighter) sets up an instability on the electrophoresis front in A^-. The opposite is the case for the electrophoresis front in B^-, where

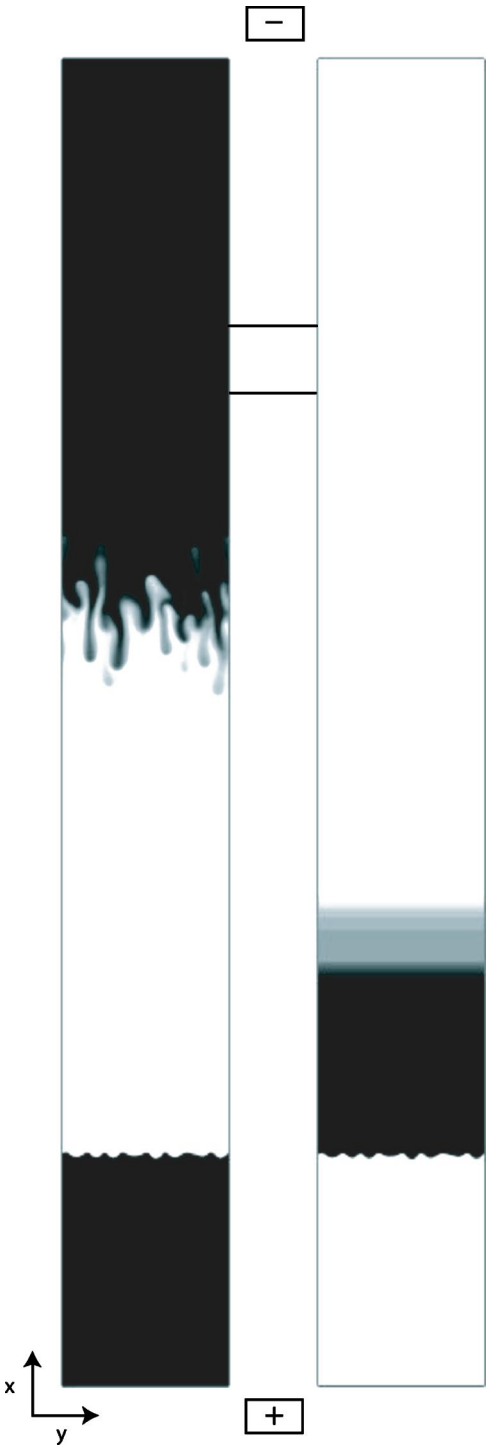

FIG. 12. Gray-level plots of a and b for $E=-3.0$ at time $t=300$, with $\beta=5.0$, $D=2.0$, $\gamma_1=1$, and $\gamma_2=0.5$. The horizontal lines indicate the initial position of the fronts. Grey levels range from white ($a=b=0$) to black ($a=1$; $b=b_s$). For this large negative value of E, both the upper electrophoretic front in a and the lower reaction front are unstable.

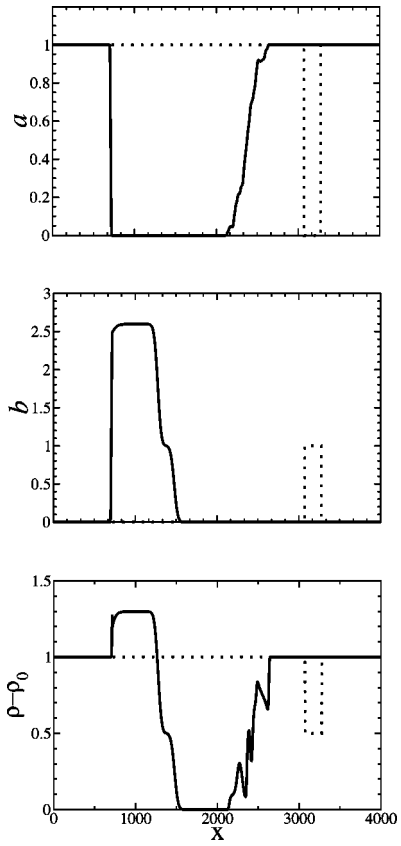

FIG. 13. Transverse averaged profile of concentrations a, b and of the density excess $\rho-\rho_o$ at time $t=300$ corresponding to the gray-level plots shown in Fig. 12.

light fluid is above heavier, and this front remains stable, see Fig. 12. These strong fields produce a high concentration of B^- at their rear and, from Eq. (25), can make $\delta\rho$ negative (with b_s sufficiently large). This gives a situation where heavy fluid is now above lighter fluid and an instability can develop on the downward-propagating front. This change in stability of a downward-propagating front is a novel feature of our system and is a direct consequence of applying electric fields.

Finally, we assess the correspondence between the instability development in our model system and in the experiments using the arsenous acid-iodate reaction [20]. In order to do so, values of the relevant dimensionless parameters for the experimental situation need to be determined. The representative value of $\gamma_2/\gamma_1=0.5$ used in the model analysis is directly related to the values of the expansion coefficients measured for arsenous acid-iodate reaction system [34]. For the calculation of β from Eq. (14), a value for the density change $\Delta\rho$ has to be chosen. There are several possibilities to choose from: (i) the estimated value of $\Delta\rho=0.36$ kg m^{-3} calculated from measured values of γ_1 and γ_2 [34], (ii) the value $\Delta\rho=0.2$ kg m^{-3} suggested in Ref. [4], and (iii) the experimental value $\Delta\rho=0.1$ kg m^{-3} measured by Ref. [34] as the difference between the densities of the fully reacted and unreacted reaction mixtures. Since the compositions of reaction mixtures used in Ref. [34] and in [20] are very similar, we took the last of these values for $\Delta\rho$ as the most probable and determined $\beta=6$. The values of the remaining quantities in Eq. (14) are $g=10$ m s^{-2}, $\mu=10^{-3}$ kg m^{-1} s^{-1} (water), $D_A=D_{IO_3^-}=1.4\times10^{-9}$ m^2 s^{-1}, $D_B=D_{I^-}=2.04\times10^{-9}$ m^2 s^{-1}, and $a_0=[IO_3^-]_0=5.0\times10^{-3}$ M. The rate constant $k_0=k_2[H^+]^2$ results from the Dushman-Roebuck kinetic scheme assuming the arsenous acid-excess case [22] which, for typical concentrations of $[H^+]=6\times10^{-3}$ M and using $k_2=10^8$ M^{-4} s^{-1}, gives $k_0=3.6\times10^3$ M^{-2} s^{-1}. The dimensionless E was calculated from Eq. (14) by considering that the quantity $\mathcal{E}$ is related to the applied electric field intensity E_{exp} through $\mathcal{E}=(F/RT)E_{exp}$ [19]. Here F and R are Faraday's and gas constants and T is the absolute temperature. The experimental values of E_{exp}, leading to the clearly observable changes in finger development, ranged from 1.5 to 3 V/cm, which correspond to values of E between 0.75 and 1.5.

Although the values of parameters D, γ_2/γ_1, and β estimated for the experimental system coincide well with those used in our model, there are distinct differences in the electric field effects on the front stability depending on whether small (up to $|E|\simeq0.3$) or larger fields are used. Weak positive (negative) electric fields were found to have the same stabilizing (destabilizing) effects on the ascending front in both the model and arsenous acid-iodate systems [20]. As in the model system, the effects on the arsenous acid-iodate front stability were assessed through dispersion relations. These curves, evaluated from experimental data, showed, as in the model, the decrease (increase) in the range of unstable wave numbers of upward-propagating fronts in a positive (negative) electric field and the respective decrease (increase) in the growth rates. Nevertheless, the electric-field-induced changes in the growth rates in the experimental system were found to be less pronounced than in the model.

The effects of larger negative electric fields in both experimental and model systems were found to diverge. While in the model the stronger negative fields ($E<-0.355$) cause the ascending front to break up into two electrophoretic fronts, see Figs. 10 and 12, this is not the case for the arsenous acid-iodate system. In this case, a front still propagates as a reaction-diffusion front. However, the effect of the electric field is to alter the reaction stoichiometry within the front and the final products of reaction, with now iodine arising as a final product [16]. The cutoff field is approximately $E_{exp}=-1$ V/cm [16], corresponding to the dimensionless value of $E=-0.5$. Thus, at larger negative fields, the reaction within the front changes from the arsenous acid excess case and the kinetic scheme can no longer be approximated by cubic autocatalysis. Consequently, the predictions obtained in our model system cannot be applied to the behavior of the arsenous acid-iodate system in these larger electric fields.

In the model, larger negative fields (in the sense defined in Fig. 1) were found to destabilize descending fronts (see Figs. 12 and 13). It should be noted that, since descending fronts propagate in this configuration towards the positive electrode, cubic autocatalysis is still an appropriate approximation of the arsenous acid-iodate reaction kinetics within the front [16] and the model predictions can be applied to the experimental system. However, the destabilization of descending fronts was not observed in the experimental system. Since the electric field used in the experiments

($|E_{exp}|=3$ V/cm giving $|E|=1.5$) is weaker than the field predicted in the model ($E=-3.0$), the possibility of destabilizing a descending front in the arsenous acid-iodate system by large negative fields remains open.

ACKNOWLEDGMENTS

The authors wish to thank Serafim Kalliadasis for helpful advice on the linear stability analysis and for providing a code for computing the dispersion curves. The authors also thank ESF programme REACTOR. H.S. and J.H.M. wish to thank the Royal Society for a Joint Project Grant. J.D. is supported by FRIA (Belgium). A.D. thanks FRFC and Prodex for financial support. H.S. thanks the Ministry of Education of the Czech Republic (Research Project No. MSM223400007) for financial support and A.Z. would like to acknowledge the support of Grant No. GACR 104/03/H141.

[1] T. A. Gribschaw, K. Showalter, D. L. Banville, and I. R. Epstein, J. Phys. Chem. **85**, 2152 (1981).
[2] A. Hanna, A. Saul, and K. Showalter, J. Am. Chem. Soc. **104**, 3838 (1982).
[3] A. Saul and K. Showalter, in *Oscillations and Traveling Waves in Chemical Systems*, edited by R. J. Field and M. Burger (Wiley-Interscience, New York, 1985).
[4] J. A. Pojman, I. R. Epstein, T. J. McManus, and K. Showalter, J. Phys. Chem. **95**, 1299 (1991).
[5] J. Masere, D. A. Vasquez, B. F. Edwards, J. W. Wilder, and K. Showalter, J. Chem. Phys. **98**, 6505 (1994).
[6] D. A. Vasquez, J. W. Wilder, and B. F. Edwards, J. Chem. Phys. **98**, 2138 (1993).
[7] I. P. Nagy, A. Keresztessy, J. A. Pojman, G. Bazsa, and Z. Noszticzius, J. Phys. Chem. **98**, 6030 (1994).
[8] M. R. Carey, S. W. Morris, and P. Kolodner, Phys. Rev. E **53**, 6012 (1996).
[9] M. Böckmann and S. C. Müller, Phys. Rev. Lett. **85**, 2506 (2000).
[10] D. Horváth, T. Bánsági, Jr., and Á. Tóth J. Chem. Phys. **117**, 4399 (2002).
[11] A. De Wit, Phys. Rev. Lett. **87**, 054502 (2001).
[12] A. De Wit, Phys. Fluids **16**, 163 (2004).
[13] J. Yang, A. D'Onofrio, S. Kalliadasis, and A. De Wit, J. Chem. Phys. **117**, 9395 (2002).
[14] S. Kalliadasis, J. Yang, and A. De Wit, Phys. Fluids **16**, 1395 (2004).
[15] L. Forštova, H. Ševčíková, M. Marek, and J. H. Merkin, Chem. Eng. Sci. **55**, 233 (2000).
[16] L. Forštova, H. Ševčíková, M. Marek, and J. H. Merkin, J. Phys. Chem. **104**, 9136 (2000).
[17] D. Šnita, H. Ševčíková, M. Marek, and J. H. Merkin, Proc. R. Soc. London, Ser. A **453**, 2325 (1997).
[18] D. Šnita, J. Lindner, M. Marek, and J. H. Merkin, Math. Comput. Modell. **27**, 1 (1998).
[19] J. H. Merkin, H. Ševčíková, D. Šnita, and M. Marek, IMA J. Appl. Math. **60**, 1 (1998).
[20] A. Zadrazil, T. Godula, and H. Ševčíková, in Proceedings of the 30th International SSChE Conference, Tatranske Matliare, Slovakia, May 2003 (Slovak University of Technology, Bratislava, 2003), on CD-ROM, paper no. R-7.
[21] H. Ševčíková and S. C. Müller, Phys. Rev. E **60**, 532 (1999).
[22] J. H. Merkin and H. Ševčíková, Phys. Chem. Chem. Phys. **1**, 91 (1999).
[23] D. Horváth, V. Petrov, S. K. Scott, and K. Showalter, J. Chem. Phys. **98**, 6332 (1993).
[24] L. Forštova, H. Ševčíková, and J. H. Merkin, Phys. Chem. Chem. Phys. **4**, 2236 (2002).
[25] D. Horváth and K. Showalter, J. Chem. Phys. **102**, 2471 (1995).
[26] A. Tóth, D. Horváth, and W. van Saarloos, J. Chem. Phys. **111**, 10 964 (1999).
[27] D. Horváth, A. Tóth, and K. Yoshikawa, J. Chem. Phys. **111**, 10 (1999).
[28] A. B. Tayler, *Mathematical Models in Applied Mechanics*, Oxford Applied Mathematics and Computing Science Series (Clarendon Press, Oxford, 1986).
[29] J. H. Merkin and H. Ševčíková, J. Math. Chem. **25**, 111 (1999).
[30] *LAPACK Users' Guide*, 3rd ed. (SIAM, Philadelphia, 1999).
[31] H. Ševčíková and M. Marek, Physica D **13**, 379 (1984).
[32] I. Z. Kiss and J. H. Merkin (unpublished).
[33] A. Malevanets, A. Careta, and R. Kapral, Phys. Rev. E **52**, 4724 (1995).
[34] O. Inomoto (private communication).
[35] C. T. Tan and G. M. Homsy, Phys. Fluids **31**, 1330 (1988).
[36] G. M. Homsy, Annu. Rev. Fluid Mech. **19**, 271 (1987).
[37] J. Fernandez, P. Kurowski, P. Petitjeans, and E. Meiburg, J. Fluid Mech. **451**, 239 (2002).